Biomaterials 86 (2016) 11–20

Contents lists available at ScienceDirect

Biomaterials

journal homepage: www.elsevier.com/locate/biomaterials

Response of MAPK pathway to iron oxide nanoparticles *in vitro* treatment promotes osteogenic differentiation of hBMSCs

Qiwei Wang [a, b], Bo Chen [a, b], Meng Cao [a, c], Jianfei Sun [a, b], Hao Wu [a, b], Peng Zhao [a], Jing Xing [a], Yan Yang [a], Xiquan Zhang [d], Min Ji [a, b], Ning Gu [a, b, *]

[a] State Key Laboratory of Bioelectronics, Jiangsu Key Laboratory of Biomaterials and Devices, School of Biological Science and Medical Engineering, Southeast University, Nanjing 210096, PR China
[b] Collaborative Innovation Center of Suzhou Nano Science and Technology, Suzhou 215123, PR China
[c] School of Public Health, Southeast University, Nanjing 210009, PR China
[d] Nanjing Chia-tai Tianqing Pharmaceutical Co. Ltd, Nanjing 210038, PR China

ARTICLE INFO

Article history:
Received 10 December 2015
Received in revised form
2 February 2016
Accepted 2 February 2016
Available online 3 February 2016

Keywords:
MAPK pathway
Iron oxide nanoparticles
Mesenchymal stem cells
Osteogenic differentiation
Regenerative medicine

ABSTRACT

Iron oxide nanoparticles (IONPs) are generally used in multiple biomedical applications. The tissue repair effect of IONPs had been demonstrated in the previous studies of our group, but the underlying mechanism is unclarified. It is well known that stem cell-based therapies show promising prospect in tissue engineering and regenerative medicine, however, whether IONPs could modulate stem cell fate to promote tissue repair is still unclear. Herein, we found that IONPs could promote osteogenic differentiation of human bone-derived mesenchymal stem cells (hBMSCs) *in vitro*. To insightfully understand the molecular mechanisms, we performed systematic analyses by use of gene microarray assay and bioinformatics analysis, which revealed that gene expression was widely regulated and classical mitogen-activated protein kinase (MAPK) signal pathway was activated by IONPs treatment. As a result, downstream genes of this pathway were regulated to promote osteogenic differentiation. In summary, the present study elucidates a molecular basis explaining how IONPs effect on hBMSCs, which could have many meaningful impacts for stem cells application in regenerative medicine.

© 2016 Elsevier Ltd. All rights reserved.

1. Introduction

Mesenchymal stem cells (MSCs) are typically considered capable of differentiation to fibroblasts, osteoblasts, chondrocytes and adipocytes et al. [1]. They could be isolated from bone marrow, adipose tissue or peripheral blood conveniently, and expanded *ex vivo* rapidly under the appropriate condition [2]. Therefore, autologous MSCs are ideal candidates in regeneration medicine and tissue engineering [3–5].

Manipulation of stem cell fate is one of the most essential aspects in developing new biomaterials and nanotechnologies for tissue engineering [6,7]. Recent studies have described that substrates with different nano-topographically patterns (nano-grooves, nano-protrusions or nano-fibrous) could induce variations in focal adhesion formation, cytoskeleton organization or cellular expansion, thus the differentiation direction of stem cell was also altered, for example, osteogenic or adipogenic [8–14]. Another study reported that nanoscale mechanical stress could drive MSCs into osteoblasts [15], both FAK and RUNX2 were activated by stress-mediated cellular force isotropy to regulate osteogenic differentiation. Gold nanoparticles (AuNPs) could also promote osteogenic differentiation of MSCs through stress-activated *p38* MAPK pathway, moreover, AuNPs with diverse charge and moiety would induce differential cell response on MSCs [16,17]. Although these potential applications were proved helpful in modulating differentiation of MSCs, little was reported to illuminate the underlying molecular mechanisms which driving those differentiations.

IONPs have been frequently used in magnetic-induction hyperthermia for cancer therapy, *in vivo* imaging, drug delivery and cell tracking [18–22]. Our previous study suggested that IONPs were capable of repairing myocardial injury, and it might be functioned by developing gap junctional crosstalk among the cardiac MSCs (cMSCs), which was revealed by another recent study [23,24]. We also reported that scaffolds composed of γ-Fe_2O_3

* Corresponding author. State Key Laboratory of Bioelectronics, Jiangsu Key Laboratory of Biomaterials and Devices, School of Biological Science and Medical Engineering, Southeast University, 2 Sipailou, Nanjing 210096, PR China.
E-mail address: guning@seu.edu.cn (N. Gu).

http://dx.doi.org/10.1016/j.biomaterials.2016.02.004
0142-9612/© 2016 Elsevier Ltd. All rights reserved.

nanoparticles, hydroxyapatite nanoparticles (nHA) and poly-lactide acid (PLA) possessed bone repair effect both *in vivo* and *in vitro* [25,26]. Meanwhile, another study suggested that the magnetic field-induced assemblies of γ-Fe_2O_3 nanoparticles could promote the differentiation of primary mouse bone marrow cells into osteoblasts [27], it indicated that the bone repair effect of IONPs was introduced by accelerating cellular osteogenesis. It has been described that dexamethasone-induced osteogenic differentiation of hBMSCs was inhibited after a pre-incubation with IONPs for one hour [28], and the inhibition was attributed to intracellular free iron that leached from IONPs. However, few investigation has been focus on the direct biological effects of IONPs themselves in bone repair and/or cellular osteogenesis.

Because osteogenic differentiation of MSCs was one of the basic processes in bone regeneration [29], the purpose of this present work is to evaluate the osteogenic differentiation of hBMSCs induced by IONPs, and illustrate the possible pathways *via* genomic studies and molecular biology assays. Taken together, these findings would provide evidences to improve the application of IONPs in regeneration medicine and understand the insightful molecular mechanism for cellular effects of IONPs in molecular level.

2. Materials and methods

2.1. Synthesis of IONPs

The polyglucose-sorbitol-carboxymethyether (PSC) coat of IONPs was modified from dextran and prepared by our laboratory. IONPs was synthesized by a modified method according to the classic chemical co-precipitation method using ferrous chloride hexahydrate and ferrous chloride tetra-hydrate (Sigma–Aldrich, MO, US) as precursors [30]. In brief, 0.2 g PSC was dissolved in 10 mL of deionized water, then a mixture of 0.06 g $FeCl_3$ and 0.03 g $FeCl_2$ dissolved in 15 mL of deionized water was added in. This mixture was cooled to 5 °C, and 1 g 28% (w/v) ammonium hydroxide was added with stirring for over 2 min. The mixture was heated at 80 °C for 1 h and purified with five cycles of ultrafiltration against deionized water using a 100 kDa membrane.

2.2. Characterization of IONPs

The prepared IONPs were primary characterized by TEM (JEM-200CX, JEOL, Japan). TEM samples were prepared by placing a few drops of the aqueous dispersions on carbon coated copper grids and drying at room temperature. The hydrodynamic diameters of IONPs were measured by dynamic light scattering (DLS) with a particle size analyzer (Malvern Zetasizer Nano ZS90, UK). The hysteresis loop of IONPs was measured by vibrating sample magnetometer (LS 7307-9309, Lakeshore Cryotronic, US). The final concentrations of iron in aqueous solution and cells were determined by phenanthroline spectrophotometry assay.

2.3. Cell culture

Primary hBMSCs were purchased from Cyagen Biosciences Inc. (CA, US) and grown at 37 °C in a humidified incubator with 5% (v/v) CO_2 in DMEM (Gibco, BRL, US) supplied with 10% (v/v) fetal bovine serum (FBS, Gibco), antibiotics (100 U/mL streptomycin and 100 U/mL penicillin) and 1% (w/v) glutamine. To maintain self-renew and multiple differentiation potential, cells were cultured at appropriate confluence (70%–80%) and harvested by 0.25% (w/v) trypsin-ethylene diamine tetra-acetic acid (EDTA) solution. All experiments were performed before the tenth passage.

2.4. Detection of cellular uptake of IONPs

Cells were seeded in 24-well plate (5×10^4 cells per well) and incubated with IONPs at different final concentration (10, 50, 100, 300, 500 μg/mL), then harvested after 24, 48 and 72 h. After ultrasonication, cell lysates were digested by 20% (w/v) HCl at 60 °C for 4 h to degrade IONPs, and then mixed with 10% (w/v) hydroxylamine hydrochloride and 0.1% (w/v) 1,10-Phenanthroline aqueous solution for 10 min, then optical density (OD) at 560 nm was detected with a micro volume spectroscopy (Nano Photometer, NP80, Implen, Germany).

Cells were fixed with 4% (v/v) formaldehyde, Perl's blue staining assay was performed to determine internalization of IONPs and nuclear fast red solution was used to stain the nucleus, then cells were observed and imaged by a microscopy (Axiovert 40, Zeiss, Germany).

2.5. Cell viability assay and apoptosis assay

CCK-8 assay was used to measure cell viability. Cells were seeded in 96-well plate (1×10^4 cells per well) and grown overnight, and then incubated with IONPs at different final concentration (concentration 10, 50, 100, 300, 500 μg/mL). After 4, 12 and 24 h incubations, cells were washed twice with PBS, CCK-8 reagent (KeyGEN, China) was added to each well and co-incubated with cells for 4 h at 37 °C. The OD of each well at 450 nm (for soluble dye) and 650 nm (for viable cells) were detected.

Annexin V-FITC/propidium iodide (PI) assays were performed for analyzing apoptosis with flow cytometry (FCM) according to the manufacturer's protocol. Briefly, 1×10^5 cells were collected and stained with apoptosis assay kit (KeyGEN, China) for 15 min at room temperature avoiding light. The apoptotic cells were analyzed with FCM (FACS Calibur, BD, USA).

2.6. ALP activity assay and alizarin red S (ARS) staining assay

Cells were seeded in 24-well plate (5×10^4 cells per well), then treated with several concentration of IONPs (final concentration 10, 50, 100, 300 μg/mL) or osteogenic induction supplement containing 5.0 mM β-glycerophosphate, 50 μg/mL ascorbic acid and 0.1 μM dexamethasone (Sigma–Aldrich, MO, US). Fresh medium was changed every two days. For ALP activity assay, cells were harvested after 7, 10, 14 days, and lysed by three cycles of freeze and thaw, the supernatants were subjected to ALP activity and total protein quantification measurement by an ALP activity kit (Beyotime Biotechnology, China) and a BCA assay kit (Beyotime Biotechnology, China). For ARS staining, cells were fixed after 14, 18 and 21 days, then stained with 40 mM ARS (pH 4.2) for 30 min at room temperature. After washed twice, cells were observed and imaged to determine formation of mineralized matrix nodules. Quantification of mineralized rate was performed by measuring the absorbance at 570 nm after eluted the ARS deposit with 10% (v/v) cetylpyridinium chloride (Sigma–Aldrich, MO, US).

2.7. Scanning electron microscope (SEM) assay for cells

Cell morphology with or without the treatment of 100 μg/mL IONPs was observed and imaged by SEM after 7 days co-incubation, as described in detail [31]. Fresh medium was changed every two days. Briefly, MSCs were soaked in the modified Karnovsky fix buffer at 4 °C overnight and post-fixed for 1 h at 4 °C with 1% (v/v) osmium tetroxide before dehydration with increasing concentrations of ethanol. Then dehydrated MSCs were maintained in desiccators for overnight air drying, SEM imaging was performed on an SEM system (Ultra Plus, Zeiss, Germany).

2.8. RNA isolation and quantitative PCR (Q-PCR)

Cells were seeded in 6-well plate (1×10^5 cells per well) and grown overnight, incubated with IONPs (final concentration 100 μg/mL) for 7 days, fresh medium was changed every two days, then harvested with trypsin-EDTA. Total RNA was isolated from cells using Trizol (Invitrogen, US) according to the manufacturer's protocols and converted into cDNA with reverse transcriptase. For Q-PCR, All reactions were triplicate and performed in 20 μL reaction volume containing cDNA, primers and SYBR-green mix (Takara, Japan). PCR was processed in ABI Step one plus Q-PCR system with following procedure: a 10 min denaturation step at 95 °C followed by 40 cycles of 15 s at 95 °C and 60 s at 60 °C. The gene-specific primers information is shown in Table S3. The relative quantification of gene expression was determined by $2^{-\Delta\Delta T}$ method.

2.9. Microarray experiment

For construction of the mRNA expression profile microarray, 10 μg of cDNAs were labeled with Cy5-dCTP and purified, then hybridized to an Agilent whole human genome oligo microarray which contained 27958 specific probes. Both IONPs-treated group and negative control group were repeated twice, therefore, four arrays were performed. After hybridization, these microarrays were washed several times, then scanned and imaged by Agilent array scanner (G2565CA), then Agilent Feature Extraction software (version 10.7) was used to extract data.

2.10. Bioinformatics analysis

Normalization and variation analysis of data was done by Agilent GeneSpring software, data were extracted and filtered as up or down regulated mRNAs according to 2-folds change, Cluster 3.0 software was used to do cluster analysis. Subsequently, to deeply explore the potential molecular mechanisms involved, prominently affected genes were enriched with KEGG pathways (http://www.genome.jp/kegg/).

2.11. Western blotting analysis and antibodies list

Cells were harvested after treated with IONPs (final concentration 100 μg/mL) for 7 days, and fresh medium was changed every two days. Then lysed by the protein extraction buffer, the supernatants were mixed with loading buffer containing SDS, dithiothreitol and bromophenol blue. After boiled for 10 min, proteins were separated by 10% SDS-PAGE and then transferred to a PDVF membrane (Millipore, MA, US), membrane was blocked in 5% (w/v) non-fat powdered milk in TBST for one hour at room temperature and probed with diluted primary antibody at 4 °C overnight. After washing three times, the membrane was then incubated with diluted horseradish peroxidase (HRP)-labeled secondary antibody for 1 h at room temperature. The protein level was detected by using the enhanced chemiluminescent (ECL) detection systems and imaged by a CCD camera.

Rabbit anti human RUNX2 (41746), BMP2 (40648), ENG (32940), CD44 (40702), MEK1/2 (41137), p-MEK1/2 (S217/S221) (11205), ERK (40903), p-ERK1/2 (T202/Y204) (12082), p90RSK (33139), p-p90RSK (T573) (11665), GAPDH (41549) and HRP-labeled goat anti rabbit IgG (L3012-2) were provided by Signalway Antibody LLC. (MD, US). Rabbit anti human OMD (ab154249) was purchased from Abcam biotechnology (UK).

2.12. Statistical analysis

All data were presented as mean ± SD of more than three independent experiments. Differences of group versus control were examined with one way ANOVA by SPSS software (version 19.0), probability less than 0.05 was considered to be statistically significant. Graphs were generated using Microsoft Excel 2013 or Origin Pro (version 8.0).

3. Results and discussion

3.1. Physicochemical properties of prepared IONPs

In current study, the aqueous dispersion of IONPs was prepared by chemical co-precipitation method as described previously [30]. Our as-prepared IONP was consist of a γ-Fe_2O_3 core and a PSC shell (Fig. 1a). Beside, PSC was modified from dextran, which is one of commonly applied stabilizers and biocompatible agents for IONPs synthesis. As a result, the probability of leaching free iron was lower, and moreover, the occurrence of idiosyncratic and allergic reactions could be reduced evidently (data not shown). Furthermore, we detected the hysteresis loop of IONPs (Fig. 1b), data showed the as-prepared IONPs were super-paramagnetic.

The physicochemical properties of IONPs investigated in this study were summarized in Table 1, which including their hydrodynamic size, polydispersity index (PDI), saturation magnetization and T_2 relaxation constant. The hydrodynamic diameters of particles were measured by DLS, the mean size was about 30.15 nm. Additionally, the transmission electron microscopy (TEM) image presented that the as-prepared IONPs dispersed quite uniformly (Fig. 1c), and we observed the mean particle size was about 7 nm. The hydrodynamic size of these NPs by intensity was larger than the value measured by TEM, probably because of the extension of PSC molecular chain and the thickness of hydrated shell. The prepared IONPs were used for the cellular internalization measurement and further biocompability assessment.

3.2. Internalization and biocompability of IONPs

The fates of IONPs in hMSCs were systematically studied by synchrotron radiation-based techniques in previous study [32]. In current study, to investigate the cellular uptake of IONPs, we employed the phenanthroline spectrophotometry assay for the quantification of iron in the cell lysates after 24–72 h co-incubation. The results revealed that IONPs were absorbed by hBMSCs in time- and dose-dependent manner (Fig. 2a). To observe the internalization of IONPs more directly, Perl's blue staining assay was employed. The results presented that more nanoparticles were internalized into the cells following longer time and higher dosage treatment (Fig. 2b). Interestingly, we noticed that the morphology of hBMSCs transformed significantly after IONPs treatment for 72 h (final concentration 100, 300 μg/mL), it implied that early differentiation of hBMSCs might have been occurred.

To evaluate the biocompability of IONPs, we performed the cell viability assay to examine the acute cytotoxicity. Cells were treated with various concentrations of IONPs for 4, 12 and 24 h, and then processed for CCK-8 incubation to determine cell viability. As it could be seen in Fig. 2c, IONPs had little toxic effect on MSCs in a time- and dose-dependent manner. Cells possessed a viability of more than 85% at all tested dosage and time points. After 24 h exposure, the viability decreased by 6.12% and 8.64% at iron concentrations 100 and 300 μg/mL, respectively. We also employed Annexin V/PI apoptosis assay to evaluate the long term toxicity of IONPs. Results in Fig. S1 showed that viable cells ratio decreased in small range with the increasing IONPs dosage and incubating time. Taken these results into account, IONPs might be a considerable biomaterial for promoting differentiation owing to their inducing potential and low cytotoxicity under the suitable concentration.

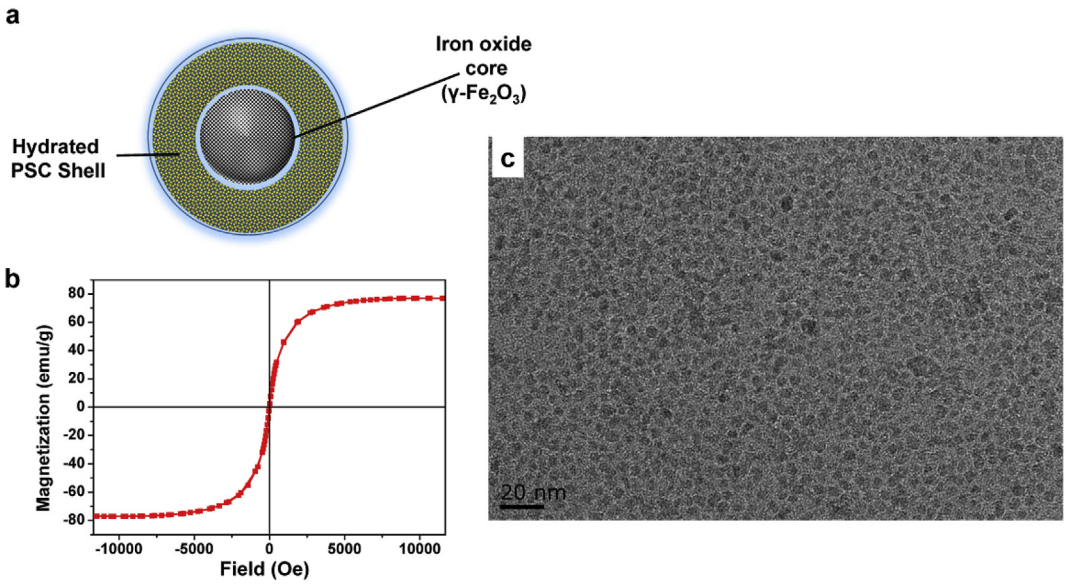

Fig. 1. Characterizations of prepared-IONPs. (a) Schematic structure of IONP. (b) Hysteresis loop of IONPs. (c) TEM image of IONPs.

Table 1
Main parameters of as-synthesized IONPs.

Sample	Hydrodynamic size (nm)	Polydispersity Index (PDI)	Saturation magnetization (emu/g)	T_2 relaxation constant (mM^{-1} s^{-1})
IONPs	30.15 ± 0.1843	0.158 ± 0.016	77	97.8

3.3. Promotion of osteogenesis by IONPs in vitro treatment

Osteogenesis of hBMSCs was examined after *in vitro* exposure of IONPs. Firstly, the increasing alkaline phosphatase (ALP) activity is an indispensable character in early stage of osteogenesis (about 7–14 days) [33–35]. Our data presented that ALP activity was dose-dependent at final concentration from 10 to 100 μg/mL, while it

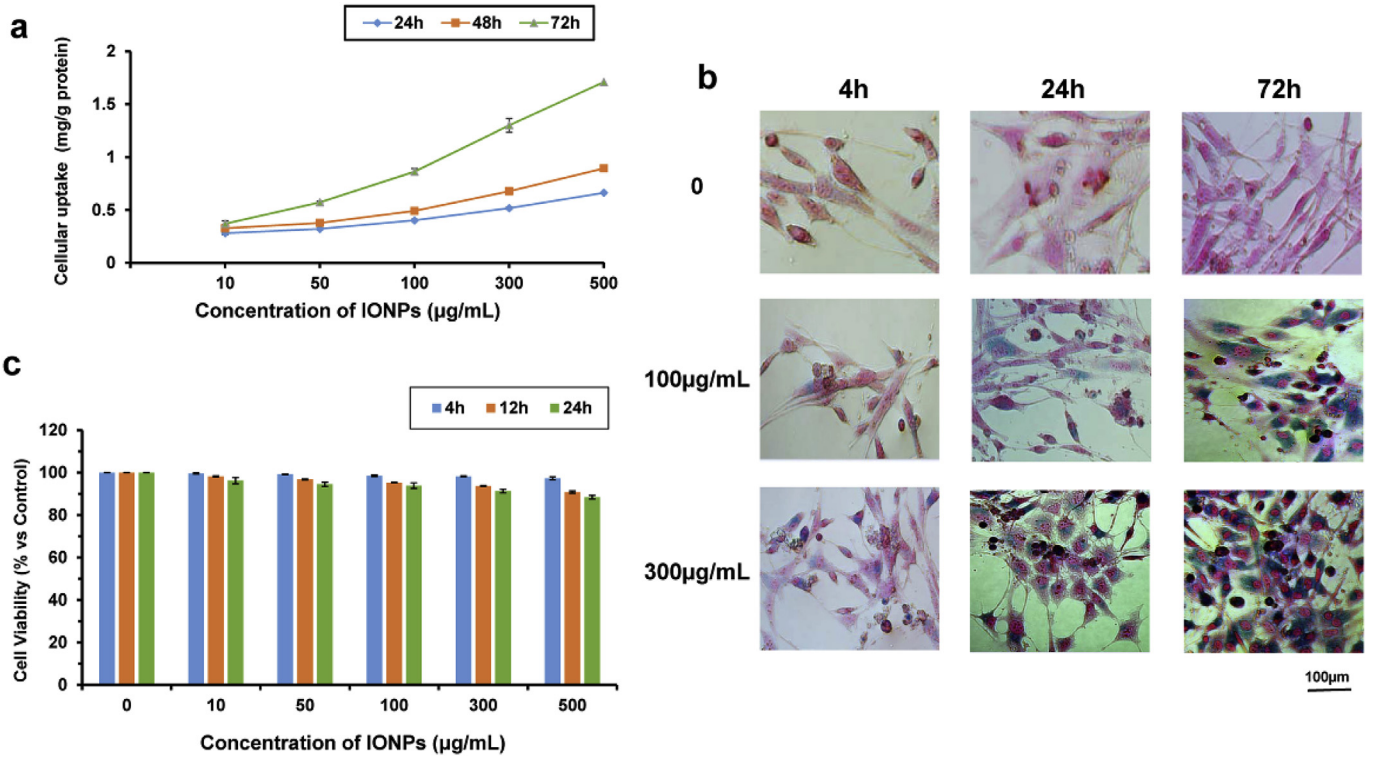

Fig. 2. Internalization and cytotoxicity of IONPs. (a) Quantify of intracellular iron contents after IONPs treatment for different concentration and time. (b) Perl's blue staining image of IONPs-treated hBMSCs. The morphology of hBMSCs changed significantly after treated with 100 and 300 μg/mL IONPs for 72 h. Scale bar: 100 μm. (c) Cell viability was detected by CCK-8 assay after treated for 4–24 h at different concentrations, data were normalized to control group (no IONPs exposure). All bars represent mean ± SD. (For interpretation of the references to colour in this figure legend, the reader is referred to the web version of this article.)

showed no obvious promotion at 300 μg/mL compared with 100 μg/mL (Fig. 3a). It suggested that 100 μg/mL might be the suitable dosage in promoting osteogenic differentiation. Meanwhile, the ALP activity was also time-dependent. As shown in Fig. 3a, ALP activity raised significantly in day 14, which is nearly the same extent as for the cells treated by osteogenesis inducing supplements (OS).

Secondly, in the later stage that MSCs turned into mature osteoblasts, extracellular bone matrix was synthesized and secreted, hence mineralized nodule formation was a typical phenotype to identifying osteoblasts [29,35]. ARS staining was performed to detect mineralized nodules. Significantly, it revealed IONPs showed a positive effect on the mineralization (Fig. 3b and c). Massive mineralized nodules were formed and stained red when hBMSCs (the sixth passages) was treated by either IONPs (100 and 300 μg/mL) or OS for 21 days (Fig. 3b). The formation of mineralized nodules was further quantified *via* eluting the ARS deposition and measuring the absorbance at 570 nm. As it shown in Fig. 3c, about 20% growth was quantified for day 14 to day 21. These results suggested that the transformation from MSCs to mature osteoblasts might have been completed in day 21.

Thirdly, the morphological variation of hBMSCs during IONPs treatment was observed by SEM (Fig. 4) and it displayed similar results to the optical microscope images (Fig. 2b). Cells presented the normal phenotype in the basal medium which could be described as spindly and fibroblast-like (Fig. 4a–d). In the medium either containing OS or IONPs, the morphology of cells became polygonal (Fig. 4e and g), more organized filopodia and depositing matrix on the cell surface were observed under higher resolution (Fig. 4f and h).

Lastly, it has been proved that several markers were inevitably expressed abnormally during the course of osteogenesis [35–37]. To acquire more concrete proofs that IONPs promoted osteogenic differentiation, we examined the reported osteogenic markers including ALPL (ALP liver), RUNX2 (runt-related transcription factor 2, also known as CBFA1), BMP2 (bone morphogenetic protein 2), OMD (osteomodulin), FOXO1 (forkhead box O1) and ATF4 (activating transcription factor 4) *via* Q-PCR experiment (Fig. 3d). The mRNA expression level of these markers were up-regulated by 4–12 folds under IONPs exposure. Western blot assay was also performed to detected protein expression level of RUNX2, BMP2 and OMD, the results revealed that protein expression level of these genes were also up-regulated when treated with 50 or 100 μg/mL IONPs *in vitro* (Fig. 3f). Subsequently, MSC markers including MCAM (melanoma cell adhesion molecule), ENG (endoglin), CLCF1 (cardiotrophin-like cytokine factor 1), TPM1 (tropomyosin 1) and CD44 were further detected (Fig. 3e and f), the mRNA expression of these genes were down-regulated by 2.5–5 folds, and the protein level of ENG and CD44 were reduced as well. All the above mentioned results suggested that pluripotent hBMSCs turned into osteoblasts when exposed to IONPs *in vitro*.

3.4. Global gene expression profile analysis of IONPs-treated hBMSCs

We further investigated the possible molecular mechanisms involved in our experiment system. Gene expression profile microarray assay was employed to compare the differences of mRNA transcripts expression level between negative control group and IONPs incubation group (100 μg/mL for 7 days). We found that 2092 up-regulated genes and 1631 down-regulated genes were detected (folds change ≥2, $p < 0.05$) under IONPs incubation. These

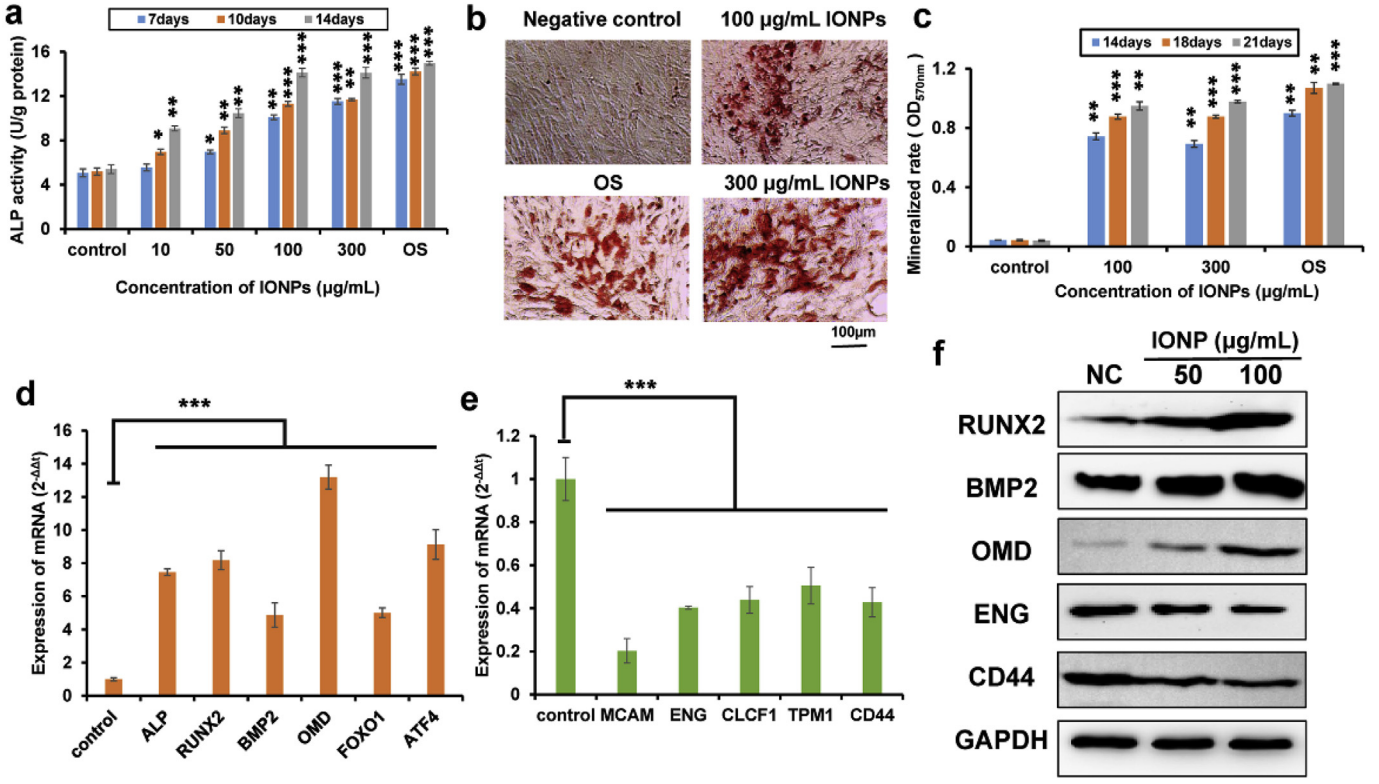

Fig. 3. Evaluation of osteogenic differentiation. (a) Effects of IONPs on the ALP activity of hBMSCs. (b) Alizarin red S staining image, hBMSCs (the sixth passages) were treated with 100 μg/mL IONPs for 21 days. OS: osteogenesis inducing supplements, scale bar: 100 μm. (c) Mineralization quantitated by elution of alizarin red S from stained mineral bone matrix. (d, e) Expression of mRNAs detected by Q-PCR after 100 μg/mL IONPs exposure for 7 days, results were determined by $2^{-\Delta\Delta T}$ method. (f) Expression of protein level detected by western blot after 50 and 100 μg/mL IONPs exposure for 7 days. All bars represent mean ± SD, n = 3, *p < 0.05; **p < 0.01; ***p < 0.001.

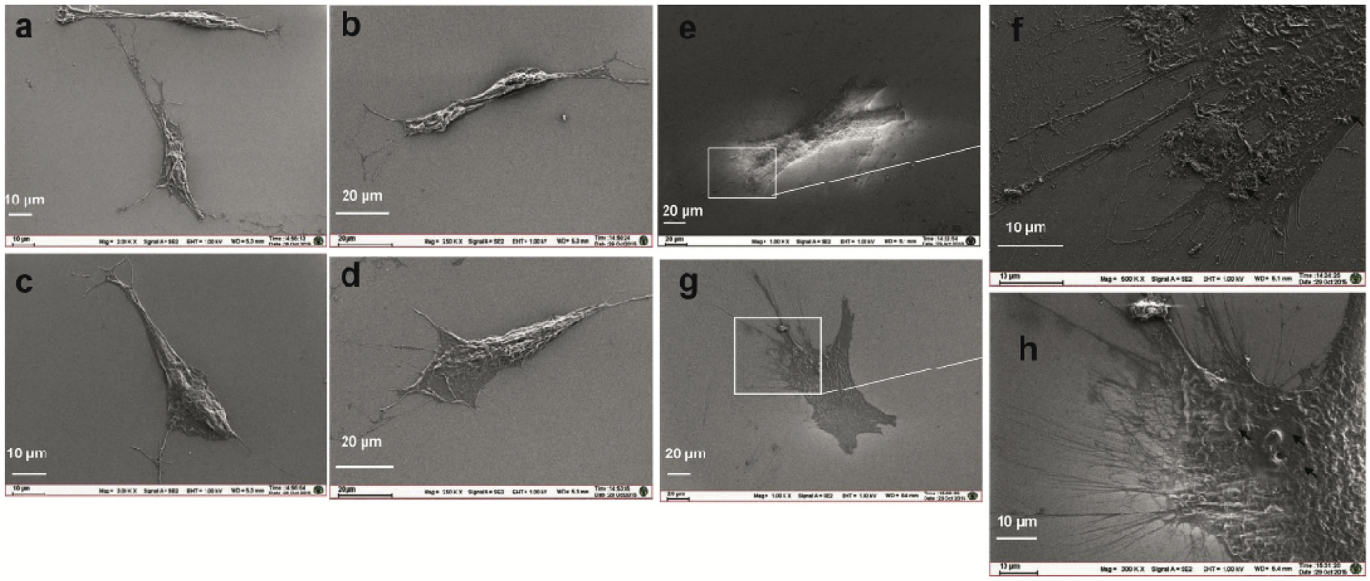

Fig. 4. SEM image of hBMSCs after 7 days culture. (a–d) hBMSCs were cultured in the absence of IONPs. (e, f) hBMSCs were cultured in the medium containing OS. (g, h) hBMSCs were treated with 100 μg/mL IONPs. Black arrows represent the depositing matrix on cell surface. All images are representative of three repeated experiments.

up- and down-regulated genes were presented as a two-dimensional hierarchical map by Treeview software (Fig. 5).

3.5. Response of MAPK signal pathway in IONPs-treated hBMSCs

Kyoto Encyclopedia of Genes and Genomes (KEGG) pathway, a database for extracting related molecular pathways from large-scale datasets generated by high-throughput experiment [38], was further employed to identify related pathways and acquire the comprehensive molecular mechanisms about IONPs-promoted osteogenesis. The results indicated that three activated pathways ($p < 0.05$) were enriched (Table S1), and MAPK signaling pathway was focused due to its function in controlling cell differentiation by regulating related downstream genes. We found 55 differentially expressed genes which containing 33 up-regulated genes and 22 down-regulated genes were involved in this pathway (Fig. 6 and Table S2). These genes were distributed in almost all cascades of the pathway, for example, receptor tyrosine kinases (RTKs, such as FGFR, PDGFR), Ras, MAPKKK (such as Tpl2/Cot, also known as MAP3K8), MAPKK (such as MEK2, also known as MAP2K2) and other kinases (such as p90RSK, also known as RPS6K). Our study indicated that MAPK signaling pathway was responded to IONPs exposure.

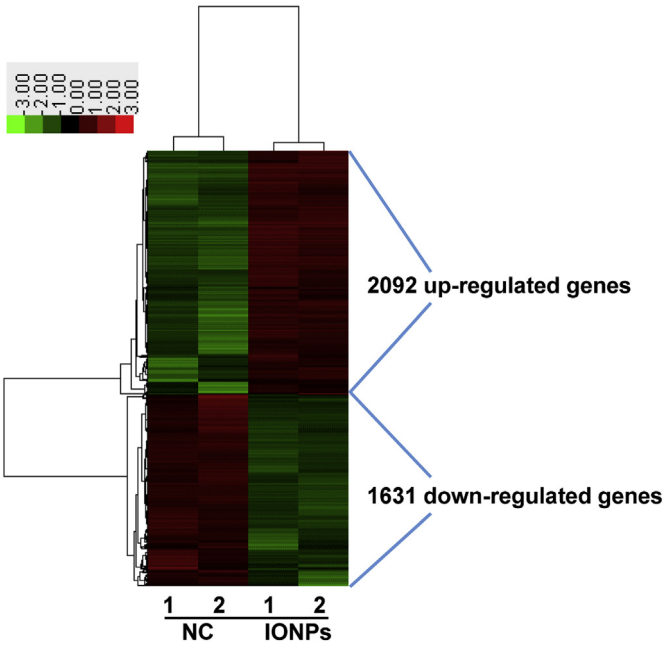

Fig. 5. Two-dimensional hierarchical clustering analysis of gene expression profile between control group and IONPs incubation group (100 μg/mL for 7 days), n = 2. Each row represented an mRNA, red: higher expression, green: lower expression. (For interpretation of the references to colour in this figure legend, the reader is referred to the web version of this article.)

For further validation of the roles of MAPK pathway in our experiment system, we performed a quantitative analysis for the genes involved in classical MAPK signaling pathway, including FGFR1 (fibroblast growth factor receptor 1), KRAS (Kirsten rat sarcoma viral oncogene homolog), MAP3K8 (Tpl2/Cot), MAP2K2 (MEK2), RPS6KA1 (ribosomal protein S6 kinase, 90 kDa, polypeptide 1) and RPS6KA3 (Fig. 7a). The results showed high consistent with microarray, mRNA level of FGFR1, KRAS, MAP3K8 (Tpl2/Cot), RPS6KA1 (p90RSK1) and RPS6KA3 (p90RSK3) were all up-regulated for about 4–11 folds, whereas MAP2K2 (MEK2) was down-regulated for about 4 folds. These results suggested that majority members of classical MAPK pathway were influenced and expressed abnormally.

3.6. Molecular mechanism for activated classical MAPK pathway in modulating osteogenic differentiation of hBMSCs

To determine whether the cascade of classical MAPK pathway was activated, the phosphorylation events were detected. We examined the substrate of MAP3K8 (Tpl2/Cot), MAP2K2 (MEK2) and ERK (phosphorylated MEK1/2, ERK1/2 and p90RSK, respectively) using the phosphorylated protein primary antibodies. As shown in Fig. 7b, phosphorylated form of MEK1/2, ERK1/2 and p90RSK were all increased obviously, although MEK1/2 was down-expressed (Fig. 7a and b) and ERK1/2 was not changed significantly

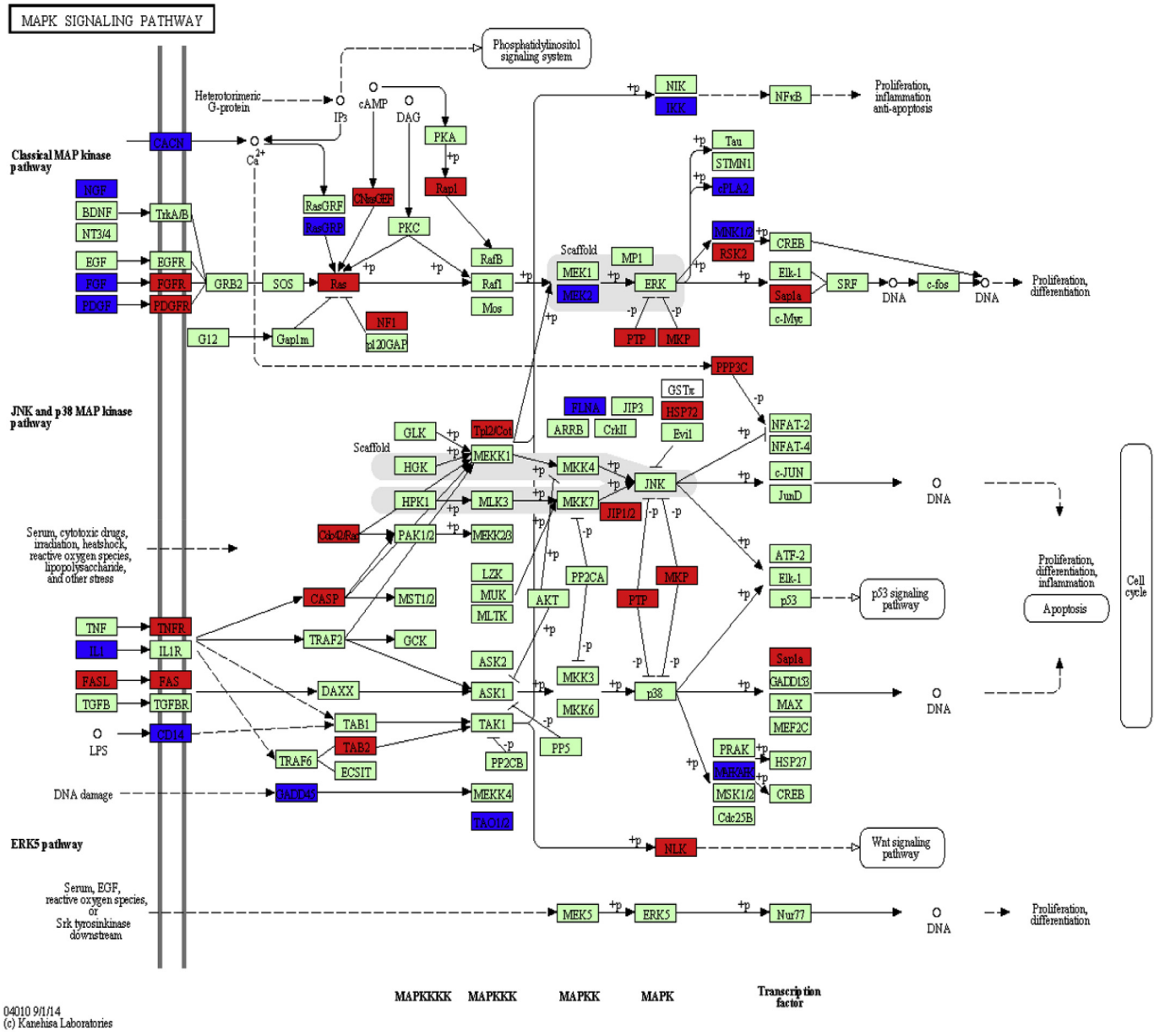

Fig. 6. MAPK signal pathway (From http://www.kegg.jp/kegg/pathway.html), red: up-regulated genes, blue: down-regulated genes. (For interpretation of the references to colour in this figure legend, the reader is referred to the web version of this article.)

(Figs. 6 and 7b). For further confirmation of the role of classical MAPK pathway, we performed ALP activity assay to detect whether the osteogenesis level could be changed by the inhibition of this pathway. For this purpose, U0126 and FR180204 (specific inhibitors of MEK and ERK, respectively) was used. We found that IONPs-promoted osteogenic differentiation was significantly blocked (Fig. S2). On the basis of these above results, we concluded that classical MAPK pathway was activated during IONPs incubation, and subsequent downstream genes that associated with osteogenic differentiation (such as BMP2, RUNX2, FOXO1 et al.) were up-regulated (Fig. 3d and f).

BMP2 is a signal molecule of TGF-β super family and plays a pivotal role during bone morphogenesis by activating Smads pathway or interacting with Wnt pathway to up-regulate osteogenic genes [39,40]. RUNX2, an indispensable gene that determines osteogenic lineage from MSCs, is a transcription factor modulated by MAPK pathway and can also up-regulated by BMP2-activated Smads pathway, and previous study reported that RUNX2 has already been used in gene therapy of bone repair [41–45]. The over-expressed RUNX2 subsequently up-regulates osteoblast marker genes such as ALPL, collagenase and osteocalcin et al. [46,47]. Thus, MSCs was driven towards osteoblasts.

In brief, the starting process in controlling the fate of MSCs can be either physical or biochemical [7,10,15,48]. Initially, different stimuli existing in intra/extracellular micro-environment (such as stress, magnetic field, chemical factors et al.) would be sensed *via* receptors, cellular membrane or cytoskeleton [33,49–51]. Then chromosomal responses which affect gene expression and protein synthesis should be evoked, alterations of crucial proteins would be resulted in differentiation of MSCs [36,52,53]. In other words, the genomic response is the crucial and direct factor in modulating differentiation of MSCs.

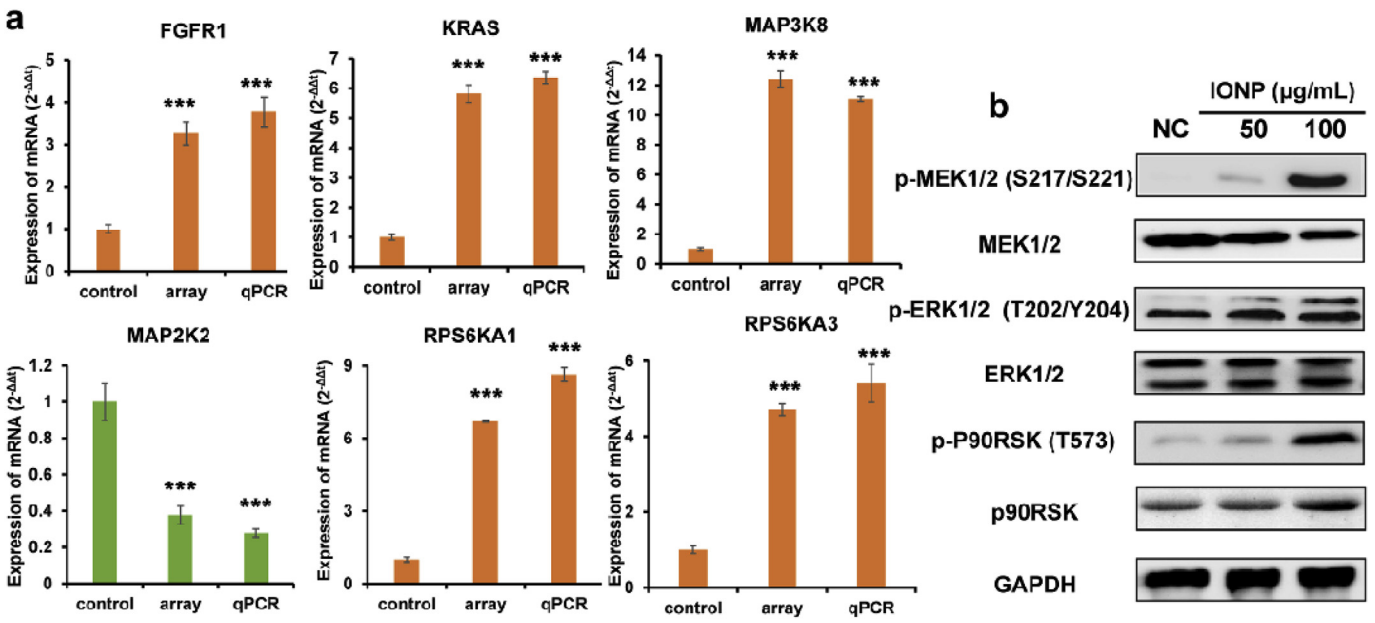

Fig. 7. Detection of genes involved in classical MAPK signal pathway. (a) Expression of mRNAs detected by Q-PCR after 100 μg/mL IONPs exposure 7 days, results were determined by $2^{-\Delta\Delta T}$ method. All bars represent mean ± SD, n = 3, $^{***}p < 0.001$. (b) Expression of the total protein level and the phosphorylated protein form, detected by western blot analysis after 50 and 100 μg/mL IONPs exposure 7 days, activation of classical MAPK pathway was induced by IONPs exposure.

In this current study, we showed the promotion effect of IONPs on the osteogenic differentiation of hBMSCs. Earlier study has demonstrated that IONPs showed inhibitory effect to dexamethasone-induced osteogenic differentiation after a pre-incubation to MSCs [28]. However, the existence of IONPs in our experiment system was the main factor of promoting osteogenic differentiation. The mechanical stress signals in promoting osteogenic differentiation might be produced in the beginning of the interaction between cell membrane and IONPs. After subsequently cellular internalization, another stimulation that promoting osteogenesis would be produced. As a whole, the consecutive signals were required, either physical or biochemical, rather than a pre-incubation. However, it was still unclarified which kinds of stimulation were produced during adsorption and internalization of IONPs. Yi et al. hypothesized that mechanical stress was produced when AuNPs interact with the cell membrane, and resulted

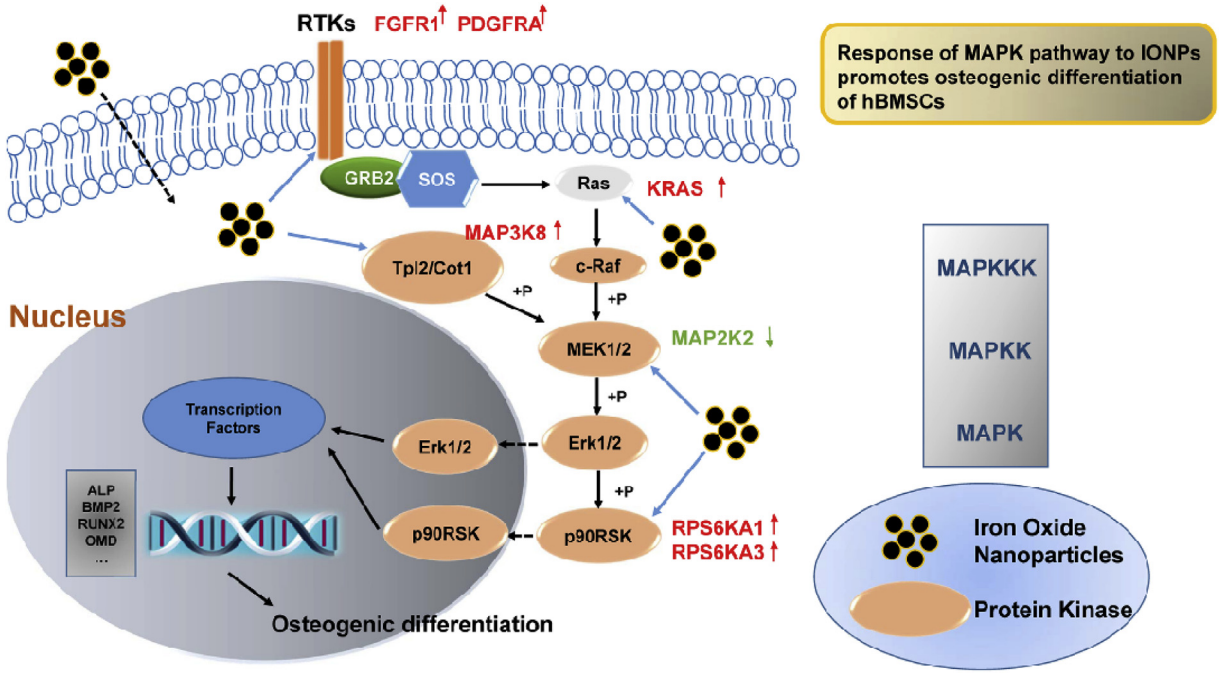

Fig. 8. Schematic illustration of IONPs-promoted osteogenic differentiation. Classical MAPK signal pathway was activated when IONPs internalized into cells, a dozen of osteogenic genes were regulated by this activation. Thus, osteogenic differentiation was promoted subsequently.

in the activation of *p38* MAPK pathway, leaded to the osteogenic differentiation of MSCs [16]. Several evidences suggested stress could be transmitted to nuclear area *via* intracellular membrane system or cytoskeleton and leaded to nucleic stretch, thus chromosomal responses and subsequent downstream signaling events were evoked immediately [15,49,53]. Actually, mechanical stress cannot be ignored. Nevertheless, nearly all biological effects of nanomaterial to cells were systematic and multifactorial [54,55], which suggested that other physical or biochemical stimuli were also existed inevitably. For instance, residual magnetism of internalized IONPs might lead a magneto-genetic response *via* so-called intracellular magneto-receptors [56]. Recent study suggested that IONPs could accelerate cell cycle progression and promote cell growth of hBMSCs, owing to their ability to diminish intracellular H_2O_2 [57]. Therefore, reactive oxygen species (ROS) and free electron which produced during iron metabolism might affect membrane potential and transmembrane transport, then differentiations might be brought out in this case.

Furthermore, the molecular mechanisms of cellular responses to those other stimuli were poorly understood, and controlling of these stimuli was necessary to manipulate stem cell fate. Moreover, JNK and *p38* MAPK pathway were also responded to IONPs treatment according to our results (Fig. 6), whether JNK and p38 MAPK pathway were activated and what role did these pathways play in IONPs promoted osteogenesis are needed to study additionally.

4. Conclusion

According to these above data, a schematic was proposed to describe our hypothesis (Fig. 8). On the whole, our data provided strong support for the conclusion that IONPs could promote the osteogenic differentiation of hBMSCs, classical MAPK pathway was activated to regulated downstream events that closely related to osteogenesis. The results revealed how IONPs contributed in modulating stem cell fate, which will also be an important basis for novel approach of therapies in bone tissue engineering and regenerative medicine.

Conflict of interest

The authors declare no competing financial interest.

Acknowledgments

This work was supported by grants from the National Key Basic Research Program of China (2011CB933503 and 2013CB934400), the National High Technology Research and Development Program ("863" Program) of China (2013AA032205), the National Natural Science Foundation of China (NSFC) for Key Project of International Cooperation (61420106012), the Natural Science Foundation of Jiangsu Province BK20130608, the Graduate Research and Innovation Program of Jiangsu Province in China (KYLX15-0167). We thank Signalway Antibody LLC for providing antibodies.

Appendix A. Supplementary data

Supplementary data related to this article can be found at http://dx.doi.org/10.1016/j.biomaterials.2016.02.004.

References

[1] M.F. Pittenger, A.M. Mackay, S.C. Beck, R.K. Jaiswal, R. Douglas, J.D. Mosca, et al., Multilineage potential of adult human mesenchymal stem cells, Science 284 (1999) 143–147.
[2] E.M. Horwitz, P.L. Gordon, W.K. Koo, J.C. Marx, M.D. Neel, R.Y. McNall, et al., Isolated allogeneic bone marrow-derived mesenchymal cells engraft and stimulate growth in children with osteogenesis imperfecta: implications for cell therapy of bone, Proc. Natl. Acad. Sci. U. S. A. 99 (2002) 8932–8937.
[3] A.I. Caplan, S.P. Bruder, Mesenchymal stem cells: building blocks for molecular medicine in the 21st century, Trends Mol. Med. 7 (2001) 259–264.
[4] D.G. Phinney, D.J. Prockop, Concise review: mesenchymal stem/multipotent stromal cells: the state of transdifferentiation and modes of tissue repair–current views, Stem Cells 25 (2007) 2896–2902.
[5] V. Mundra, I.C. Gerling, R.I. Mahato, Mesenchymal stem cell-based therapy, Mol. Pharm. 10 (2013) 77–89.
[6] W.L. Murphy, T.C. McDevitt, A.J. Engler, Materials as stem cell regulators, Nat. Mater. 13 (2014) 547–557.
[7] S. Martino, F. D'Angelo, I. Armentano, J.M. Kenny, A. Orlacchio, Stem cell-biomaterial interactions for regenerative medicine, Biotechnol. Adv. 30 (2012) 338–351.
[8] E.K. Yim, E.M. Darling, K. Kulangara, F. Guilak, K.W. Leong, Nanotopography-induced changes in focal adhesions, cytoskeletal organization, and mechanical properties of human mesenchymal stem cells, Biomaterials 31 (2010) 1299–1306.
[9] K. Kulangara, Y. Yang, J. Yang, K.W. Leong, Nanotopography as modulator of human mesenchymal stem cell function, Biomaterials 33 (2012) 4998–5003.
[10] J. Yang, L.E. McNamara, N. Gadegaard, E.V. Alakpa, K.V. Burgess, R.M. Meek, et al., Nanotopographical induction of osteogenesis through adhesion, bone morphogenic protein cosignaling, and regulation of microRNAs, ACS Nano 8 (2014) 9941–9953.
[11] Y. Wang, R. Gao, P.P. Wang, J. Jian, X.L. Jiang, C. Yan, et al., The differential effects of aligned electrospun PHBHHx fibers on adipogenic and osteogenic potential of MSCs through the regulation of PPARgamma signaling, Biomaterials 33 (2012) 485–493.
[12] Z. Yin, X. Chen, J.L. Chen, W.L. Shen, T.M. Hieu Nguyen, L. Gao, et al., The regulation of tendon stem cell differentiation by the alignment of nanofibers, Biomaterials 31 (2010) 2163–2175.
[13] M.J. Biggs, R.G. Richards, N. Gadegaard, C.D. Wilkinson, R.O. Oreffo, M.J. Dalby, The use of nanoscale topography to modulate the dynamics of adhesion formation in primary osteoblasts and ERK/MAPK signalling in STRO-1+ enriched skeletal stem cells, Biomaterials 30 (2009) 5094–5103.
[14] S. Watari, K. Hayashi, J.A. Wood, P. Russell, P.F. Nealey, C.J. Murphy, et al., Modulation of osteogenic differentiation in hMSCs cells by submicron topographically-patterned ridges and grooves, Biomaterials 33 (2012) 128–136.
[15] H. Nikukar, S. Reid, P.M. Tsimbouri, M.O. Riehle, A.S. Curtis, M.J. Dalby, Osteogenesis of mesenchymal stem cells by nanoscale mechanotransduction, ACS Nano 7 (2013) 2758–2767.
[16] C. Yi, D. Liu, C.C. Fong, J. Zhang, M. Yang, Gold nanoparticles promote osteogenic differentiation of mesenchymal stem cells through p38 MAPK pathway, ACS Nano 4 (2010) 6439–6448.
[17] J.J. Li, N. Kawazoe, G. Chen, Gold nanoparticles with different charge and moiety induce differential cell response on mesenchymal stem cell osteogenesis, Biomaterials 54 (2015) 226–236.
[18] L.Y. Chien, J.K. Hsiao, S.C. Hsu, M. Yao, C.W. Lu, H.M. Liu, et al., In vivo magnetic resonance imaging of cell tropism, trafficking mechanism, and therapeutic impact of human mesenchymal stem cells in a murine glioma model, Biomaterials 32 (2011) 3275–3284.
[19] J. Xie, Y. Zhang, C. Yan, L. Song, S. Wen, F. Zang, et al., High-performance PEGylated Mn-Zn ferrite nanocrystals as a passive-targeted agent for magnetically induced cancer theranostics, Biomaterials 35 (2014) 9126–9136.
[20] C. Xu, D. Miranda-Nieves, J.A. Ankrum, M.E. Matthiesen, J.A. Phillips, I. Roes, et al., Tracking mesenchymal stem cells with iron oxide nanoparticle loaded poly(lactide-co-glycolide) microparticles, Nano Lett. 12 (2012) 4131–4139.
[21] J. Duan, J. Dong, T. Zhang, Z. Su, J. Ding, Y. Zhang, et al., Polyethyleneimine-functionalized iron oxide nanoparticles for systemic siRNA delivery in experimental arthritis, Nanomedicine (Lond) 9 (2014) 789–801.
[22] P. Yi, G. Chen, H. Zhang, F. Tian, B. Tan, J. Dai, et al., Magnetic resonance imaging of Fe3O4@SiO2-labeled human mesenchymal stem cells in mice at 11.7 T, Biomaterials 34 (2013) 3010–3019.
[23] F. Xiong, H. Wang, Y. Feng, Y. Li, X. Hua, X. Pang, et al., Cardioprotective activity of iron oxide nanoparticles, Sci. Rep. 5 (2015) 8579.
[24] J. Han, B. Kim, J.Y. Shin, S. Ryu, M. Noh, J. Woo, et al., Iron oxide nanoparticle-mediated development of cellular gap junction crosstalk to improve mesenchymal stem cells' therapeutic efficacy for myocardial infarction, ACS Nano 9 (2015) 2805–2819.
[25] J. Meng, Y. Zhang, X. Qi, H. Kong, C. Wang, Z. Xu, et al., Paramagnetic nanofibrous composite films enhance the osteogenic responses of pre-osteoblast cells, Nanoscale 2 (2010) 2565–2569.
[26] J. Meng, B. Xiao, Y. Zhang, J. Liu, H. Xue, J. Lei, et al., Super-paramagnetic responsive nanofibrous scaffolds under static magnetic field enhance osteogenesis for bone repair in vivo, Sci. Rep. 3 (2013) 2655.
[27] J. Sun, X. Liu, J. Huang, L. Song, Z. Chen, H. Liu, et al., Magnetic assembly-mediated enhancement of differentiation of mouse bone marrow cells cultured on magnetic colloidal assemblies, Sci. Rep. 4 (2014) 5125.
[28] Y.C. Chen, J.K. Hsiao, H.M. Liu, I.Y. Lai, M. Yao, S.C. Hsu, et al., The inhibitory effect of superparamagnetic iron oxide nanoparticle (Ferucarbotran) on osteogenic differentiation and its signaling mechanism in human mesenchymal stem cells, Toxicol. Appl. Pharmacol. 245 (2010) 272–279.
[29] G.S. Stein, J.B. Lian, Molecular mechanisms mediating proliferation/differentiation interrelationships during progressive development of the osteoblast

phenotype, Endocr. Rev. 14 (1993) 424–442.
[30] K.G. Paul, T.B. Frigo, J.Y. Groman, E.V. Groman, Synthesis of ultrasmall superparamagnetic iron oxides using reduced polysaccharides, Bioconjug Chem. 15 (2004) 394–401.
[31] S. Qi, C. Yi, S. Ji, C.C. Fong, M. Yang, Cell adhesion and spreading behavior on vertically aligned silicon nanowire arrays, ACS Appl. Mater Interfaces 1 (2009) 30–34.
[32] F. Tian, G. Chen, P. Yi, J. Zhang, A. Li, L. Zheng, et al., Fates of Fe_3O_4 and Fe_3O_4@ SiO_2 nanoparticles in human mesenchymal stem cells assessed by synchrotron radiation-based techniques, Biomaterials 35 (2014) 6412–6421.
[33] B.M. Abdallah, C.H. Jensen, G. Gutierrez, R.G. Leslie, T.G. Jensen, M. Kassem, Regulation of human skeletal stem cells differentiation by Dlk1/Pref-1, J. Bone Min. Res. 19 (2004) 841–852.
[34] S.M. Pockwinse, L.G. Wilming, D.M. Conlon, G.S. Stein, J.B. Lian, Expression of cell growth and bone specific genes at single cell resolution during development of bone tissue-like organization in primary osteoblast cultures, J. Cell. Biochem. 49 (1992) 310–323.
[35] B. Kulterer, G. Friedl, A. Jandrositz, F. Sanchez-Cabo, A. Prokesch, C. Paar, et al., Gene expression profiling of human mesenchymal stem cells derived from bone marrow during expansion and osteoblast differentiation, BMC Genomics 8 (2007) 70.
[36] A.M. Hakelien, J.C. Bryne, K.G. Harstad, S. Lorenz, J. Paulsen, J. Sun, et al., The regulatory landscape of osteogenic differentiation, Stem Cells 32 (2014) 2780–2793.
[37] H. Qi, D.J. Aguiar, S.M. Williams, A. La Pean, W. Pan, C.M. Verfaillie, Identification of genes responsible for osteoblast differentiation from human mesodermal progenitor cells, Proc. Natl. Acad. Sci. U. S. A. 100 (2003) 3305–3310.
[38] M. Kanehisa, A database for post-genome analysis, Trends Genet. 13 (1997) 375–376.
[39] X. Gao, A. Usas, Y. Tang, A. Lu, J. Tan, J. Schneppendahl, et al., A comparison of bone regeneration with human mesenchymal stem cells and muscle-derived stem cells and the critical role of BMP, Biomaterials 35 (2014) 6859–6870.
[40] S.J. Rodda, A.P. McMahon, Distinct roles for Hedgehog and canonical Wnt signaling in specification, differentiation and maintenance of osteoblast progenitors, Development 133 (2006) 3231–3244.
[41] F.S. Wang, C.J. Wang, S.M. Sheen-Chen, Y.R. Kuo, R.F. Chen, K.D. Yang, Superoxide mediates shock wave induction of ERK-dependent osteogenic transcription factor (CBFA1) and mesenchymal cell differentiation toward osteoprogenitors, J. Biol. Chem. 277 (2002) 10931–10937.
[42] J.S. Bae, S. Gutierrez, R. Narla, J. Pratap, R. Devados, A.J. van Wijnen, et al., Reconstitution of Runx2/Cbfa1-null cells identifies a requirement for BMP2 signaling through a Runx2 functional domain during osteoblast differentiation, J. Cell. Biochem. 100 (2007) 434–449.
[43] Y.F. Huang, J.J. Lin, C.H. Lin, Y. Su, S.C. Hung, c-Jun N-terminal kinase 1 negatively regulates osteoblastic differentiation induced by BMP2 via phosphorylation of Runx2 at Ser104, J. Bone Min. Res. 27 (2012) 1093–1105.
[44] Y.B. Niu, X.H. Kong, Y.H. Li, L. Fan, Y.L. Pan, C.R. Li, et al., Radix Dipsaci total saponins stimulate MC3T3-E1 cell differentiation via the bone morphogenetic protein-2/MAPK/Smad-dependent Runx2 pathway, Mol. Med. Rep. 11 (2015) 4468–4472.
[45] N. Monteiro, D. Ribeiro, A. Martins, S. Faria, N.A. Fonseca, J.N. Moreira, et al., Instructive nanofibrous scaffold comprising runt-related transcription factor 2 gene delivery for bone tissue engineering, ACS Nano 8 (2014) 8082–8094.
[46] W.G. Jang, E.J. Kim, D.K. Kim, H.M. Ryoo, K.B. Lee, S.H. Kim, et al., BMP2 protein regulates osteocalcin expression via Runx2-mediated Atf6 gene transcription, J. Biol. Chem. 287 (2012) 905–915.
[47] G. Xiao, D. Jiang, R. Gopalakrishnan, R.T. Franceschi, Fibroblast growth factor 2 induction of the osteocalcin gene requires MAPK activity and phosphorylation of the osteoblast transcription factor, Cbfa1/Runx2, J. Biol. Chem. 277 (2002) 36181–36187.
[48] D.E. Discher, D.J. Mooney, P.W. Zandstra, Growth factors, matrices, and forces combine and control stem cells, Science 324 (2009) 1673–1677.
[49] Y. Sawada, M.P. Sheetz, Force transduction by Triton cytoskeletons, J. Cell Biol. 156 (2002) 609–615.
[50] L. He, D. Montell, A cellular sense of touch, Nat. Cell Biol. 14 (2012) 902–903.
[51] Y. Sawada, M. Tamada, B.J. Dubin-Thaler, O. Cherniavskaya, R. Sakai, S. Tanaka, et al., Force sensing by mechanical extension of the Src family kinase substrate p130Cas, Cell 127 (2006) 1015–1026.
[52] T. Cremer, C. Cremer, Chromosome territories, nuclear architecture and gene regulation in mammalian cells, Nat. Rev. Genet. 2 (2001) 292–301.
[53] M.J. Dalby, N. Gadegaard, P. Herzyk, D. Sutherland, H. Agheli, C.D. Wilkinson, et al., Nanomechanotransduction and interphase nuclear organization influence on genomic control, J. Cell. Biochem. 102 (2007) 1234–1244.
[54] S. Li, H. Wang, Y. Qi, J. Tu, Y. Bai, T. Tian, et al., Assessment of nanomaterial cytotoxicity with SOLiD sequencing-based microRNA expression profiling, Biomaterials 32 (2011) 9021–9030.
[55] X. Lu, H. Lu, L. Zhao, Y. Yang, Z. Lu, Genome-wide pathways analysis of nickel ion-induced differential genes expression in fibroblasts, Biomaterials 31 (2010) 1965–1973.
[56] S. Qin, H. Yin, C. Yang, Y. Dou, Z. Liu, P. Zhang, et al., A magnetic protein biocompass, Nat. Mater. 15 (2016) 217–226.
[57] D.M. Huang, J.K. Hsiao, Y.C. Chen, L.Y. Chien, M. Yao, Y.K. Chen, et al., The promotion of human mesenchymal stem cell proliferation by superparamagnetic iron oxide nanoparticles, Biomaterials 30 (2009) 3645–3651.